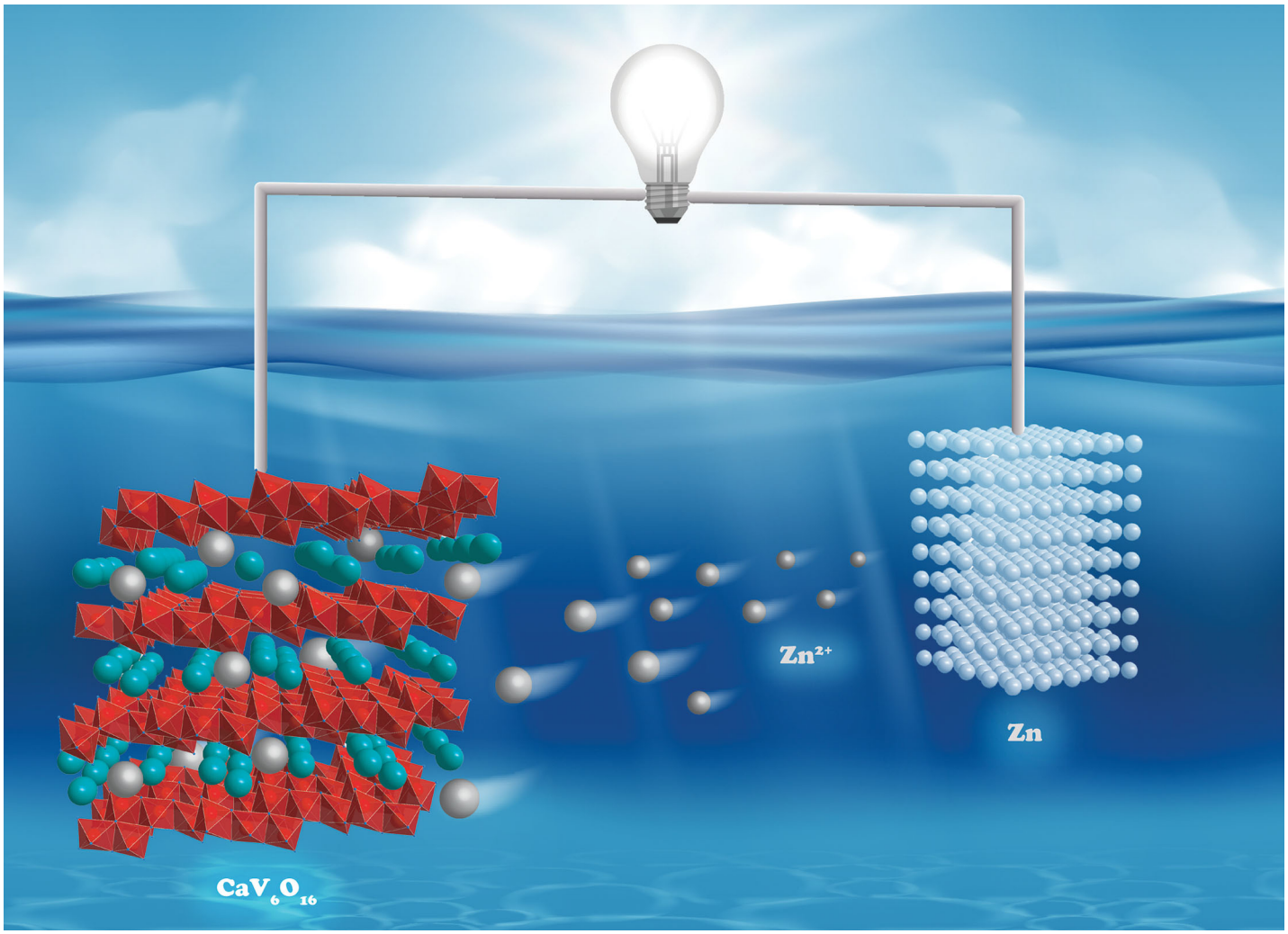

Showcasing research from Passerini's Laboratory, Helmholtz Institute Ulm (HIU), Karlsruhe Institute of Technology (KIT), Ulm, Germany

Calcium vanadate sub-microfibers as highly reversible host cathode material for aqueous zinc-ion batteries

$CaV_6O_{16}{\cdot}3H_2O$ synthesized *via* a highly efficient and fast microwave reaction is investigated as a cathode material for aqueous zinc-ion batteries. The large interlayer distance and the pillaring effect of Ca^{2+} result in the high reversibility of the Zn^{2+} insertion process, making the material a promising cation host.

As featured in:

See Arianna Moretti, Stefano Passerini *et al.*, *Chem. Commun.*, 2019, **55**, 2265.

ROYAL SOCIETY OF CHEMISTRY | Celebrating IYPT 2019

rsc.li/chemcomm

Registered charity number: 207890

ChemComm

COMMUNICATION

View Article Online
View Journal | View Issue

Cite this: *Chem. Commun.*, 2019, **55**, 2265

Received 6th September 2018,
Accepted 20th November 2018

DOI: 10.1039/c8cc07243d

rsc.li/chemcomm

Calcium vanadate sub-microfibers as highly reversible host cathode material for aqueous zinc-ion batteries†

Xu Liu,[ab] Huang Zhang,[ab] Dorin Geiger,[c] Jin Han,[ab] Alberto Varzi,[ab] Ute Kaiser,[c] Arianna Moretti*[ab] and Stefano Passerini*[ab]

For the first time, $CaV_6O_{16}\cdot 3H_2O$ (CVO), synthesized *via* a highly efficient and fast microwave reaction, is used as a cathode material for aqueous zinc-ion batteries. *Ex situ* X-ray diffraction confirms the structure of this material to be stable upon reversible Zn^{2+} intercalation, due to its large interlayer distance (8.08 Å). The pillaring effect of calcium makes the as-prepared CVO an excellent Zn^{2+} cation host.

Since their commercialization in 1991, lithium-ion batteries (LIBs) have rapidly developed, conquering the market of portable electronics and, currently, electric vehicles.[1] However, the potential cost increase due to limited supply of lithium and, especially, cobalt is pushing the interest towards alternative secondary battery chemistries relying on more abundant elements.[2] Furthermore, the commonly used carbonate-based electrolytes possess high cell voltages, however, being highly flammable and toxic and requiring stringent conditions for manufacturing, safe operation and recycling.[3] Replacing organic solvent-based electrolytes with aqueous ones is an effective strategy to overcome such drawbacks. In this context, aqueous zinc batteries (AZBs) are a promising complementary technology to LIBs. Zinc is an abundant element produced on a large-scale,[4] which, in its metallic form, can be directly used as an anode in aqueous electrolyte batteries. Having a redox potential of −0.76 V *vs.* SHE, which is comparable to those of other commonly used anode materials in aqueous systems, *e.g.* $LiTi_2(PO_4)_3$ (−0.52 V *vs.* SHE) and $NaTi_2(PO_4)_3$ (−0.6 V *vs.* SHE), but a high volumetric theoretical capacity (5854 mA h cm^{-3}), Zn is an extremely appealing anode material.[5]

Although rechargeable AZBs are appealing, they are still in their infancy and their development is hindered by the restricted choice of cathode materials that often display limited cycle life, poor rate capability, and structural instability upon multivalent cation insertion. Polyanionic compounds and Prussian blue analogues suffer from low specific capacity, while manganese-based oxides have a short lifespan due to severe manganese dissolution.[6] Nazar *et al.* reported a high-capacity and long-life rechargeable AZB based on $Zn_{0.25}V_2O_5\cdot nH_2O$.[7] Since then, a series of layered vanadium-based oxides and sulfides have been investigated.[8] In general, these compounds deliver high specific capacity (>300 mA h g^{-1}) when the composition and morphology are carefully designed. For example, as reported by Pang *et al.*, $H_2V_3O_8$ nanowires (diameter is 50–100 nm) anchored on the surface of graphene sheets exhibit a high capacity of 394 mA h g^{-1} at 100 mA g^{-1}.[9] The high specific capacity of vanadium oxides compensates for their relatively low operating voltage (around 0.8 V *vs.* Zn^{2+}/Zn). However, although displaying a better cycling stability than manganese oxides, vanadium oxides still need further improvement to meet the standard of practical use. Previous studies have shown that adopting a suitable metal cation as a pillaring agent can effectively stabilize the vanadium slab, reducing, or even fully avoiding the structural collapse upon Li^+ and Na^+ intercalation/de-intercalation.[10] This strategy was extended to AZBs and, so far, focused on the effect of alkali metal cations (*e.g.*, LiV_3O_8, $Na_{0.25}V_2O_5$, $Na_2V_6O_{16}$, KV_3O_8, $K_{0.25}V_2O_5$, $K_2V_6O_{16}$, and $K_2V_8O_{21}$),[11] while the effect of alkaline-earth metal cations was less investigated.

$CaV_6O_{16}\cdot 3H_2O$ (CVO) is a typical vanadium-bronze mineral. The calcium cations are located in the interlayer space and coordinated by oxygens from the two vanadium slabs, facing each other, and by oxygens belonging to bound water molecules (see the inset in Fig. 1).[12] Hence, the Ca cations may act as pillaring agents stabilizing the vanadium oxide structure, like the alkali metal cations do. Moreover, CVO has a larger interlayer distance compared with alkali-metal vanadium bronzes with formulae $M_xV_2O_5$, MV_3O_8, MV_6O_{15}, and $M_2V_6O_{16}$ (M = Li, Na, or K) (Table S1, ESI,† summarizes the interlayer distance of these vanadium bronzes), which favours the intercalation of the shuttling ions. Actually, CVO has been reported as a cathode for LIBs,

[a] *Helmholtz Institute Ulm (HIU), Electrochemistry I, 89081 Ulm, Germany*
[b] *Karlsruhe Institute of Technology (KIT), 76021 Karlsruhe, Germany. E-mail: stefano.passerini@kit.edu, arianna.moretti@kit.edu*
[c] *Central Facility of Electron Microscopy, Electron Microscopy Group of Materials Science, Ulm University, Albert-Einstein-Allee 11, D-89081 Ulm, Germany*

† Electronic supplementary information (ESI) available: Experimental details and supplementary figures. See DOI: 10.1039/c8cc07243d

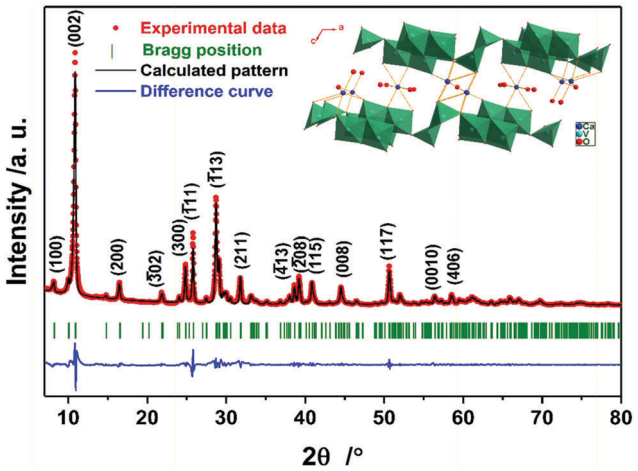

Fig. 1 Summary of the Rietveld refinement of the as-prepared CVO. The experimental data, calculated pattern, difference curve, and Bragg position are shown in red, black, blue, and olive, respectively. The inset shows the crystal structure model projected along [010].

delivering a specific capacity of 252 mA h g^{-1} at 100 mA g^{-1}, and showing no fading after 200 cycles at 200 mA g^{-1}.[13] However, to the best of our knowledge, the reversible zinc storage properties of CVO have not been studied yet. Furthermore, the reported preparation methods for CVO are complex or time-consuming, necessitating several steps to obtain CVO. For example, Zhang *et al.* used electrochemical deposition to synthesize a precursor, which, upon an additional hydrothermal treatment, led to the synthesis of CVO.[13] Li *et al.* prepared CVO *via* thermal hydrolysis of pre-prepared $Ca_{10}V_6O_{25}$.[14] Even the simplest surfactant-assisted hydrothermal method still needs the reactor to be set at 160 °C for several hours (10 h).[15]

In this communication, we report a new, very fast and highly efficient synthesis of CVO based on the microwave reaction, and explore, for the first time, its zinc storage properties in aqueous electrolyte. In our typical preparation, 1 mmol $Ca(CH_3COO)_2$ and 2 mmol V_2O_5 were mixed in 20 mL ultrapure water. Through microwave dielectric heating, CVO was obtained after only 2 h at 180 °C. Notably, only 105 seconds were needed to reach 180 °C, after which a power as low as 20 W was sufficient to keep the temperature constant (see Fig. S1, ESI†). Therefore, our method offers clear advantages over previous preparation procedures in terms of easiness and time and cost reduction. More details on the material synthesis and further processing can be found in the ESI.†

The structure of the as-prepared sample was confirmed by powder X-ray diffraction (PXRD). Fig. 1 shows the summary of the Rietveld refinement (R_{wp} = 11.14%, the obtained structural parameters are shown in Table S2, ESI†), demonstrating that the compound is phase-pure CVO, whose structure is depicted in the inset of Fig. 1. According to the refined peak position of the (002) plane, the interlayer distance is calculated to be 8.08 Å, which is much larger than those of the initial material, V_2O_5 (4.38 Å, PDF 41-1426), and other vanadium bronzes incorporating alkali metals (see Table S1, ESI†). Thermogravimetric analysis (TGA) was carried out to detect the amount of intercalated water (see Fig. S2, ESI†), which was 8.4 wt%, corresponding to the theoretical content in the formula $CaV_6O_{16}{\cdot}3H_2O$ (8.2 wt%).[13]

As seen in Fig. 2a, the as-prepared CVO was composed of uniform fibers longer than 100 μm and with a diameter in the range of hundreds of nanometers. The latter sub-micrometric dimension is certainly beneficial for shortening the solid-state diffusion path of Zn^{2+}.[16] Nevertheless, the diameter of the as-prepared CVO is still larger than those of other vanadium oxides reported for AZBs,[10] which, as discussed in the following, may affect its electrochemical performance. Additionally, the valence state of vanadium in CVO is 5+, which could result in a high electronic resistance within a single wire.[17] Fig. 2b shows the EDX elemental mapping of the CVO micro-wires. The distribution of the three elements (Ca, V, and O) in the CVO material was found to be uniform and in good agreement with the secondary electron image taken on the same region. The transmission electron microscopy (TEM) image shown in Fig. 2c further reveals that the fiber is not uniform. Furthermore, the parallel boundaries along the edge indicate that it consists of slabs. The inset displays a typical [0$\bar{1}$0] electron diffraction pattern, demonstrating that the fiber is a single crystal with the slabs stacking along the same direction. Finally, the high-resolution TEM (HRTEM) image (Fig. 2d) shows well-developed lattice fringes with an interplanar spacing of 1.08 nm, which is identical to that of the (100) plane of CVO.

The electrochemical properties of CVO were examined using Zn//CVO coin cells employing the 3 m aqueous solution of $Zn(CF_3SO_3)_2$ as the electrolyte. Further information about the cell setup and measurement conditions is reported in the ESI.†

The cyclic voltammetry (CV) profile obtained at a scanning rate of 0.05 mV s^{-1} is shown in Fig. 3a. Two pairs of reversible redox peaks, located at 0.65 V and 0.98 V in the cathodic scan (peak 1 and 2), and at 0.48 V and 0.76 V in the anodic scan (peak 3 and 4), indicate that Zn^{2+} intercalation into $CaV_6O_{16}{\cdot}3H_2O$ occurs

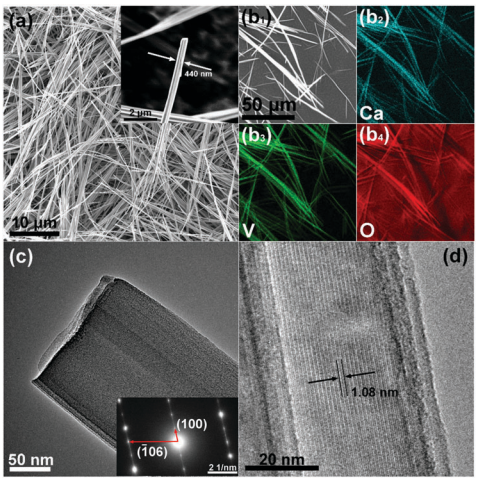

Fig. 2 (a) SEM images of the as-prepared CVO. (b) SEM image and the corresponding EDX elemental mapping images of Ca, V, and O. (c) TEM image of the as-prepared CVO and the corresponding electron diffraction pattern. (d) HRTEM image of the as-prepared CVO.

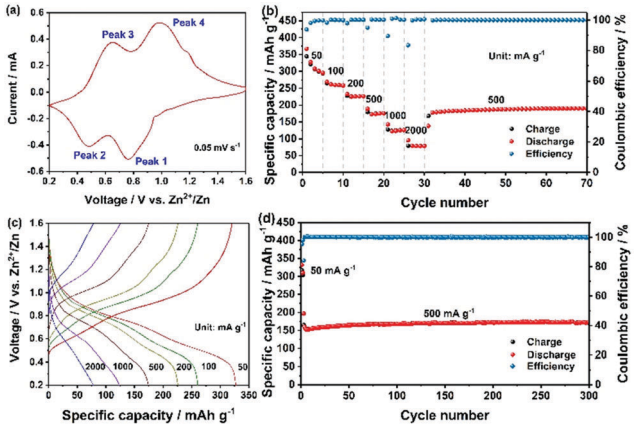

Fig. 3 Electrochemical performance of the as-fabricated CVO electrode. (a) CV curve at 0.05 mV s^{-1}. (b) Specific capacity and coulombic efficiency obtained at different current densities. (c) Charge–discharge profiles at different current densities. (d) Specific capacity and coulombic efficiency upon extensive cycling at 500 mA g^{-1}. The first two activation cycles were performed at 50 mA g^{-1}.

through a multistep process.[18] With a faster scan rate (from 0.1 to 0.5 mV s^{-1}) the peak separation increased (the voltammograms are displayed in Fig. S3a, ESI†). According to the empirical power-law relationship with the scan rate:

$$i = av^b \quad (1)$$

where i is the current, v is the scan rate, and a and b are the adjustable parameters,[17] the b values of peaks 1–4 are calculated to be 0.72, 0.75, 0.5 and 0.7, respectively.

For further details, the $\log(i)$ *vs.* $\log(v)$ curves are displayed in Fig. S3b (ESI†). These values indicate that the capacity of the as-prepared CVO is controlled by both capacitive (b = 1) and diffusive (b = 0.5) processes. Noticeably, they are lower than those reported for other layered vanadium oxides and sulfides, such as VO_2, $K_2V_6O_{16}$, V_2O_5, and VS_2, which is due to the relatively larger dimensions of CVO reducing the capacitive contribution.[11,19]

Galvanostatic discharge/charge cycles at different current densities are reported in Fig. 3b. In the first cycle at 50 mA g^{-1}, the discharge capacity reached 367 mA h g^{-1}, while the coulombic efficiency was 93.69% and gradually increased upon cycling. Since the size of the microwave synthesized CVO wires was rather large, the diffusion-controlled process is expected to be predominant. Thus, the resulting high specific capacity must result from the large interlayer distance in CVO. The irreversible capacity observed in the first cycle could arise from two possible parasitic reactions involving the reduction of dissolved O_2 and the salt anion ($CF_3SO_3^-$). In fact, although the electrolyte was de-aereated by bubbling N_2 in it for one hour, the cell was assembled in an ambient atmosphere, leading to some inevitable O_2 in the cell. The reduction of oxygen during the discharge process could consume some electrons and contribute to the irreversible capacity.[20] Regarding the salt anion, $CF_3SO_3^-$, its reduction in concentrated $NaCF_3SO_3$ electrolytes has been reported.[21] However, the efficiency rapidly increased to 99.72% at the 4th cycle, demonstrating, overall, a good reversibility of the multivalent cation intercalation process. Because of the larger grain size and, possibly, lower electronic conductivity, the specific capacity at high specific current is not superior to those of other reported vanadium oxides, leaving considerable room for optimization. Nevertheless, at a specific current of 1 A g^{-1}, a specific capacity higher than 125 mA h g^{-1} was achieved. The corresponding charge–discharge curves are shown in Fig. 3c. The plateaus matched well with the redox peaks in Fig. 3a. When the specific current was brought back to 500 mA g^{-1}, the cell recovered its capacity without any loss, implying the integrity of the CVO structure. The evaluation of the long-term cycling is displayed in Fig. 3d. At the 4th cycle, the discharge capacity was 160 mA h g^{-1}, gradually increasing to 170 mA h g^{-1} and then remaining stable for the whole duration of the test (*i.e.*, 300 cycles). The cell voltage *vs.* capacity during a few, selected charge–discharge cycles is displayed in Fig. S4 (ESI†).

The electrochemical properties of several cathode materials for AZBs are compared in Table S3 (ESI†). The specific capacity of the as-prepared CVO is much higher than that of polyanionic compounds, Prussian blue analogues, and manganese-based oxides, and it exceeds that of a series of other vanadium-based oxides as well as sulfides. Furthermore, CVO displays excellent capacity retention, *e.g.*, better than most of the reported cathode materials for AZBs.

To investigate the Zn-cation storage mechanism, the *ex situ* XRD characterization of CVO electrodes was performed. Fig. 4a displays the diffractograms obtained at different states of charge and discharge during the first cycle. The corresponding charge/discharge profile is shown in Fig. 4b. Notably, the initial interlayer distance (7.4 Å) was smaller than that of the pristine powder. This can be attributed to the partial loss of the water molecules intercalated in the interlayer due to the extensive drying process after electrode fabrication. Upon Zn^{2+} intercalation, the (002) peak gradually shifted to higher degrees, suggesting the decrease of the interlayer distance from the initial value (7.4 Å) to 6.8 Å at the fully intercalated state. This is due to

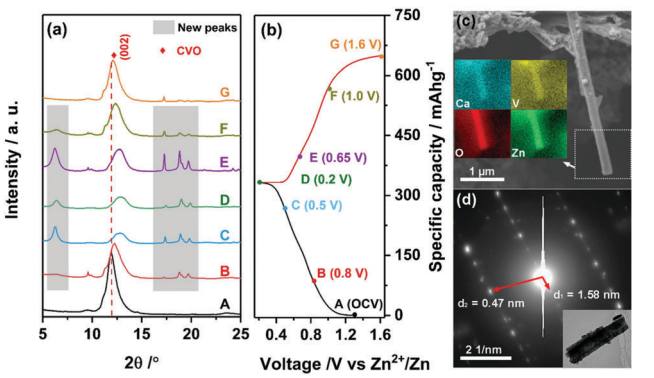

Fig. 4 (a) *Ex situ* XRD patterns of the as-fabricated CVO electrodes at various states of the first cycle, and (b) the corresponding voltage profile. (c) SEM image and the corresponding EDX elemental mapping images of the CVO fiber discharged to 0.2 V. (d) Electron diffraction pattern of the CVO fiber discharged to 0.2 V and the corresponding TEM image of the fiber.

the intercalated Zn^{2+} cations attracting the adjacent, negatively charged V–O slabs. When Zn^{2+} was extracted, the (002) peak shifted back to lower degrees. The final interlayer distance was very close to the initial value. This reveals the excellent reversibility of Zn^{2+} (de-)intercalation in the layered structure of CVO. Interestingly, a set of new peaks, marked by grey boxes in Fig. 4a, appeared during Zn^{2+} intercalation and disappeared upon Zn^{2+} release.[16] No other peaks evolved at higher angles (Fig. S5, ESI†). It is reasonable to think that these peaks originated from the intercalated Zn^{2+}. To gain more information about the intercalated CVO, SEM and TEM were applied to the fully discharged sample. As shown in Fig. 4c, the fiber-like morphology is retained. The distribution of zinc element matches well with the secondary electron image, indicating the presence of zinc in the intercalated fiber, *i.e.*, confirming the proposed intercalation mechanism. Observing the electron diffraction pattern, one can conclude that the zinc intercalated CVO fiber is a single crystal. The calculated interlayer spacings and the HRTEM image (see Fig. S6, ESI†) imply that the lattice constants have quite large difference after the intercalation of zinc. Considering the regular and reversible shift of the (002) peak during the charge/discharge process, one can infer that the intercalated compound still retains some structural features of pristine CVO. A deep analysis is ongoing to clarify the structural evolutions occurring in the CVO electrode during cell cycling.

In conclusion, ultra-long CVO micro-wires were obtained with a highly efficient and very fast microwave reaction. Owing to the large interlayer distance and pillaring effect of calcium, the electrode material reversibly intercalated up to 4.5 equivalents of Zn^{2+} per mole of CVO, delivering high specific capacity with excellent capacity retention. *Ex situ* XRD measurement confirmed the reversibility of the process, the high structural stability of CVO. Although we can already foresee further optimization of the synthesis conditions (*e.g.*, a decrease of CVO wire diameter, introduce mixed vanadium valence states or electronically conductive materials), CVO prepared by the microwave reaction is a promising cathode for aqueous zinc-ion batteries and a potential host for other multivalent cations.

X. L., H. Z., and J. H. gratefully acknowledge financial support from the China Scholarship Council (CSC). Financial support from the Helmholtz Association is also acknowledged.

Conflicts of interest

There are no conflicts to declare.

Notes and references

1 A. Moretti, F. Maroni, I. Osada, F. Nobili and S. Passerini, *ChemElectroChem*, 2015, **2**, 529.
2 C. Vaalma, D. Buchholz, M. Weil and S. Passerini, *Nat. Rev. Mater.*, 2018, **3**, 18013.
3 Z. Peng, Q. L. Wei, S. S. Tan, P. He, W. Luo, Q. Y. An and L. Q. Mai, *Chem. Commun.*, 2018, **54**, 4041.
4 X. G. Zhang, *Corrosion and Electrochemistry of Zinc*, Springer, 1996.
5 H. B. Wang, K. L. Huang, Y. Q. Zeng, S. Yang and L. Q. Chen, *Electrochim. Acta*, 2007, **52**, 3280; D. Bin, F. Wang, A. C. Tamirat, S. M. Suo, Y. G. Wang, C. S. Wang and Y. Y. Xia, *Adv. Energy Mater.*, 2018, **8**, 1703008.
6 G. L. Li, Z. Yang, Y. Liang, C. H. Jin, W. Huang, X. L. Ding and Y. H. Huang, *Nano Energy*, 2016, **25**, 211; R. Trócoli and F. L. Mantia, *ChemSusChem*, 2015, **8**, 481; S. Zhao, B. Han, D. T. Zhang, Q. Huang, L. Xiao, L. Chen, D. G. Ivey, Y. D. Deng and W. F. Wei, *J. Mater. Chem. A*, 2018, **6**, 5733.
7 D. P. Kundu, B. D. Adams, V. Duffort, S. H. Vajargah and L. F. Nazar, *Nat. Energy*, 2016, **1**, 16119.
8 M. Song, H. Tan, D. L. Chao and H. J. Fan, *Adv. Funct. Mater.*, 2018, **28**, 1802564.
9 Q. Pang, C. L. Sun, Y. H. Yu, K. N. Zhao, Z. Y. Zhang, P. M. Voyles, G. Chen, Y. J. Wei and X. D. Wang, *Adv. Energy Mater.*, 2018, **8**, 1800144.
10 J. S. Meng, Z. A. Liu, C. J. Niu, X. M. Xu, X. Liu, G. B. Zhang, X. P. Wang, M. Huang, Y. Yu and L. Q. Mai, *J. Mater. Chem. A*, 2016, **4**, 4893; Y. L. Zhao, C. H. Han, J. W. Yang, J. Su, X. M. Xu, S. Li, L. Xu, R. P. Fang, H. Jiang, X. D. Zou, B. Song, L. Q. Mai and Q. J. Zhang, *Nano Lett.*, 2015, **15**, 2180; J. H. Yao, Y. W. Li, R. C. Massé, E. Uchaker and G. Z. Cao, *Energy Storage Mater.*, 2018, **11**, 205.
11 M. H. Alfaruqi, V. Mathew, J. J. Song, S. J. Kim, S. Islam, D. T. Pham, J. Jo, S. Kim, J. P. Baboo, Z. L. Xiu, K. S. Lee, Y. K. Sun and J. Kim, *Chem. Mater.*, 2017, **29**, 1684; Y. S. Cai, F. Liu, Z. G. Luo, G. Z. Fang, J. Zhou, A. Q. Pan and S. Q. Liang, *Energy Storage Mater.*, 2018, **13**, 168; P. He, G. B. Zhang, X. B. Liao, M. Y. Yan, X. Xu, Q. Y. An, J. Liu and L. Mai, *Adv. Energy Mater.*, 2018, **8**, 1702463; V. Soundharrajan, B. Sambandam, S. Kim, M. H. Alfaruqi, D. Y. Putro, J. Jo, S. Kim, V. Mathew, Y. K. Sun and J. Kim, *Nano Lett.*, 2018, **18**, 2402; P. Hu, T. Zhu, X. P. Wang, X. J. Wei, M. Y. Yan, J. T. Li, W. Luo, W. Yang, W. C. Zhang, L. Zhou, Z. Q. Zhou and L. Q. Mai, *Nano Lett.*, 2018, **18**, 1758; B. Sambandam, V. Soundharrajan, S. Kim, M. H. Alfaruqi, J. Jo, S. Kim, V. Mathew, Y. K. Sun and J. Kim, *J. Mater. Chem. A*, 2018, **6**, 15530; B. Y. Tang, G. Z. Fang, J. Zhou, L. B. Wang, Y. P. Lei, C. Wang, T. Q. Lin, Y. Tang and S. Q. Liang, *Nano Energy*, 2018, **51**, 579.
12 M. A. Cooper, F. C. Hawthorne, V. Y. Karpenko, L. A. Pautov and A. A. Agakhanov, *J. Gersci.*, 2014, **59**, 159.
13 X. Zhang, W. W. Yang, J. G. Liu, Y. Zhou, S. C. Feng, S. C. Yan, Y. F. Yao, G. Wang, L. Wan, C. Fang and Z. G. Zou, *Nano Energy*, 2016, **22**, 38.
14 L. Li, S. Zhang, S. Wang, H. Du and Y. Zhang, *J. Wuhan Univ. Technol.*, 2014, **23**, 433.
15 L. Kong, M. Shao, Q. Xie, J. Liu and Y. Qian, *J. Cryst. Growth*, 2004, **260**, 435.
16 X. Xu, M. Y. Yan, X. C. Tian, C. C. Yang, M. Z. Shi, Q. L. Wei, L. Xu and L. Q. Mai, *Nano Lett.*, 2015, **15**, 3879.
17 H. Q. Song, C. F. Liu and C. K. Zhang, *Nano Energy*, 2016, **22**, 1; Y. W. Li, J. H. Yao, E. Uchaker, M. Zhang, J. J. Tian, X. Y. Liu and G. Z. Cao, *J. Phys. Chem. C*, 2013, **117**, 23507.
18 J. W. Ding, Z. G. Du, L. Q. Gu, B. Li, L. Z. Wang, S. W. Wang, Y. J. Gong and S. B. Yang, *Adv. Mater.*, 2018, **30**, 1800762.
19 T. Y. Wei, Q. Li, G. Z. Yang and C. X. Wang, *J. Mater. Chem. A*, 2018, **6**, 8006; P. He, M. Y. Yan, G. B. Zhang, R. M. Sun, L. N. Chen, Q. Y. An and L. Q. Mai, *Adv. Energy Mater.*, 2017, **7**, 1601920.
20 L. M. Suo, D. Oh, Y. X. Lin, Z. Q. Zhuo, O. Bordoin, T. Gao, F. Wang, A. Kushima, Z. Q. Wang, H. C. Kim, Y. Qi, W. L. Yang, F. Pan, J. Li, K. Xu and C. S. Wang, *J. Am. Chem. Soc.*, 2017, **139**, 18670–18680.
21 L. M. Suo, O. Borodin, Y. S. Wang, X. H. Rong, W. Sun, X. L. Fan, S. Y. Xu, M. A. Schroeder, A. V. Cresce, F. Wang, C. Y. Yang, Y. S. Hu, K. Xu and C. S. Wang, *Adv. Energy Mater.*, 2017, **7**, 1701189.

